Contemporary Mathematics
https://ojs.wiserpub.com/index.php/CM/

Research Article

Predator-Prey Dynamics Unveiling the Role of Harvesting and the Existence of Toxicity with Fading Memory with Neural Networking

Aziz Khan[1*], Hadeel Bin Amer[2], Ramesh K[3], Thabet Abdeljawad[1], Rajermani Thinakaran[4]

[1] Department of Mathematics and Sciences, Prince Sultan University, Riyadh 11586, Saudi Arabia
[2] Department of Computer Science, College of Computer and Information Sciences, Majmaah University, Al-Majmaah 11952, Saudi Arabia
[3] Department of Mathematics, Anurag University, Venkatapur, Hyderabad, Telangana 500088, India
[4] Faculty of Data Science and Information Technology, INTI International University, Nilai, Negeri Sembilan 71800, Malaysia
E-mail: akhan@psu.edu.sa

Received: 26 November 2025; **Revised:** 16 January 2026; **Accepted:** 13 February 2026

Abstract: In the present study, the Holling Type-II functional response is integrated with additional harvesting and toxicity parameters to investigate the overall dynamics of a Caputo fractional-order predator-prey model. In order to capture the memory effects and nonlocal dynamics present in natural systems, the model incorporates fractional-order derivatives. Incorporating harvesting and toxicity impacts into the system allows us to gain insight into their effects on population stability and coexistence. The effect of functional response saturation on predator-prey interactions is also taken into account by the interaction terms. For the numerical method validation neural network analysis is used. The results provide novel insights regarding ecological system sustainability management by highlighting the significant effects of fractional ordering, life cycle analysis, harvesting, and toxicity on predator-prey interactions.

***Keywords*:** prey-predator model, Caputo fractional order, harvesting, life cycle analysis, stability

MSC: 26A33, 34A08, 03C65

1. Introduction

In order to keep our environment safe in the modern day, environmental toxicology has become an important issue. Many forms of industrial waste, as well as toxic gas emissions, smoke, and dangerous chemicals, contribute to environmental pollution. Research into the potentially lethal impacts of man-made chemical, biological, and physical contaminants on all forms of life is known as environmental toxicology. As a branch of environmental toxicology, eco-toxicology investigates the ways in which toxicants impair ecosystems as a whole, as well as individual humans. Environmental toxicology was established in 1962 by Rachel Carson's seminal work "Silent Spring" [1], which established it as a distinct subfield of toxicology. She addressed the consequences of pesticide use that is not regulated in this area of research. The toxin can have an effect on predators, reducing their numbers and raising prey populations, or it can have the opposite effect, causing predator populations to collapse as a result of food scarcity.

One of the main concerns for bioeconomic modelling is the presence of harmful substances in the environment. The investigations of authors [2–6] and others established the foundation for the mathematical model incorporating toxic

Copyright ©2026 Aziz Khan, et al.
DOI: https://doi.org/10.37256/cm.7320269282
This is an open-access article distributed under a CC BY license
(Creative Commons Attribution 4.0 International License)
https://creativecommons.org/licenses/by/4.0/

substances. Most of the models only take into account communities of one or two species in general, not considering aquatic habitats specifically. When one species releases a toxin into the ecosystem, it impacts not only that species but also its potential growth-limiting predators. The ever-increasing demands of human beings are driving industries to release massive quantities of toxicants into the ecosystem on a daily basis. The species residing there are mostly impacted by these toxicants. Considering that the appearance of various species results in the creation of hazardous chemicals by each species, Maynard Smith [7] incorporated the consequences of poisonous compounds into a two-species Lotka-Volterra competitive system. Environmentally harmful effects of toxicants emitted by marine species have recently attracted the attention of researchers. When one species releases a toxin, it impacts not just that species but also its ability to grow. However, Ordinary Differential Equations (ODEs) are typically used to create the models. Our focus is on mathematical models derived from Caputo fractional order differential equation systems that are applicable to eco-toxicology. Since fractional order systems have several benefits, such as an infinite amount of memory [8] and the ability to offer more parameters for improved simulation, several researchers [9–12] are working in this area. Some intriguing results have been found by studying the limited number of models [13, 14] that address toxic environments in a fractional order framework. Inadequate discussion of toxicity, impacts of Caputo fractional order derivative, and harvesting in earlier models plagues their examinations of population dynamics.

Our work expands upon previous studies by introducing a Holling Type-II functional response into a predator-prey framework that does not use integer orders. For more accurate representation of predator consumption rates at densities of prey, the Holling Type-II response common in ecological models introduces saturation effects. Two important elements influencing population dynamics harvesting and toxicity are also included. Both the natural and human-caused exploitation of species, known as harvesting, and environmental degradation and pollution, or toxicity, pose serious threats to the long-term viability of ecosystems. Analysis of the impacts of toxicity, harvesting, and a non-integer order dynamics on predator-prey interactions is the main goal of this work.

This study explores a two-species fractional-order system that incorporates harvesting and is influenced by a toxic environment, as outlined in Section 2. Additionally, several key definitions and preliminary concepts have been addressed within this section. The following is the outline of the remaining parts of the paper: Solutions to the system have been proven to exist, be unique, and be bounded in Section 3. The stability of the system's conceivable stable states is covered in Section 4. Hopf bifurcation as a result of derivative order was covered in Section 5. Exciting evolutionary dynamics based on Caputo fractional order variation, toxicity effects, and harvesting on the underlying system are demonstrated in Section 6 using numerical simulations. The final section contains the conclusions.

2. Model description and preliminaries

The study of ecological habitats involves looking at places where predators and prey populations live and interact. The populations of prey and predators are experiencing logistic growth, and their interaction adheres to a Holling type II functional response. The assumption is that the predator functions as a generalist, meaning it does not rely solely on a specific prey type. This indicates that when prey is not present, it can rely on alternative resources found within the habitat for survival. Additionally, the capture for each unit effort assumption is often used to regulate prey and predator populations. The following is one way of expressing this system's behaviour:

$$\begin{aligned}\frac{dx}{dt} &= rx\left(1-\frac{x}{k_1}\right)-\frac{axy}{1+bx}-q_1E_1x,\\ \frac{dy}{dt} &= sy\left(1-\frac{y}{k_2}\right)+\frac{caxy}{1+bx}-q_2E_2y.\end{aligned} \tag{1}$$

We then present the impact of memory and toxic compounds on biological populations, assuming that external toxic substances directly harm prey and that predators indirectly absorb toxic substances through prey consumption. Consequently, the following is the reduced fractional prey-predator model:

$$D_t^{\alpha}x = rx\left(1-\frac{x}{k_1}\right)-\frac{axy}{1+bx}-q_1E_1x-d_1x^2,$$

$$D_t^{\alpha}y = sy\left(1-\frac{y}{k_2}\right)+\frac{caxy}{1+bx}-q_2E_2y-d_2y. \tag{2}$$

In this context, d_1x^2 shows how poisonous compounds affect the prey, whereas d_2y shows how they affect the predator and signifies the memory effect $(0 \leq \alpha < 1)$. The ecological importance of every component and parameter in framework (2) is explained in Table 1.

Table 1. Variables and parameters used in model (2)

Variables	Biological significance	Units
x	Size of prey population	Amount per unit area (tons)
y	Size of consumer population	Amount per unit area (tons)
r	Inherent rate of advancement of	Prey per day
s	Inherent rate of advancement of	Predator per day
k_1	Sustainable population limit of the prey	Amount per unit area (tons)
k_2	Sustainable population limit of the predator	Amount per unit area (tons)
a	Predator assault frequency on	Prey per day
b	Tackling period	Per day
c	Rate of transformation of y on x	Constant & $0 < c < 1$
q_1	Catchability rate on prey population	Per day
q_2	Catchability rate on predator population	Per day
E_1	Extraction intensity directed against the prey	Total number of vessels per day
E_2	Extraction intensity directed against the predator	Total number of vessels per day

Set $X = \frac{x}{k_1}$, $Y = \frac{y}{k_2}$, and $\tau = rt$ as the dimensionless variables. Based on this, system (2) in its non-dimensionalized form is

$$D_{\tau}^{\alpha}X = X(1-X)-\frac{\tilde{a}XY}{1+\tilde{b}X}-\tilde{q}_1X-\tilde{d}_1X^2,$$

$$D_{\tau}^{\alpha}Y = \tilde{s}Y(1-Y)+\frac{\tilde{c}\tilde{a}XY}{1+\tilde{b}X}-\tilde{q}_2Y-\tilde{d}_2Y, \tag{3}$$

involving the parameters are expressed in the form of dimensionless versions:

$$D_t^{\alpha} = r^{\alpha} D_{\tau}^{\alpha},\ \widetilde{a} = \frac{ak_2}{rk_1},\ \widetilde{b} = bk_1,\ \widetilde{q}_1 = \frac{q_1 E_1}{r},\ \widetilde{q}_2 = \frac{q_2 E_2}{s},\ \widetilde{d}_1 = \frac{d_1}{rk_1},\ \widetilde{d}_2 = \frac{d_2}{s},\ \widetilde{s} = \frac{s}{r},\ \widetilde{c} = \frac{ck_2}{k_1}.$$

Preliminaries

Definition 1 [15] Considering an expression $f \in C^n([t_0, \infty], \mathbb{R})$, it is possible to symbolise and express the Caputo fractional derivative of order α as follows: ${}_{t_0}^{C}D_t^{\alpha} f(t) = \frac{1}{\Gamma(n-\alpha)} \int_{t_0}^{t} \frac{f^{(n)}(\zeta)}{(t-\zeta)^{\alpha-n+1}} d\zeta$, in which $\Gamma(\cdot)$ is the Gamma function, $t \geq t_0$ and n is a positive integer such that $\alpha \in (n-1, n)$.

Notably, given values of α ranging from 0 to 1, ${}_{t_0}^{C}D_t^{\alpha} f(t) = \frac{1}{\Gamma(1-\alpha)} \int_{t_0}^{t} \frac{f'(\zeta)}{(t-\zeta)^{\alpha}} d\zeta$.

Definition 2 [16] The description of both single as well as double parametric Mittag-Leffler functions is as follows: $E_{\phi}(x) = \sum_{i=0}^{\infty} \frac{x^i}{\Gamma(\phi i + 1)}$ and $E_{\phi,\mu}(x) = \sum_{i=0}^{\infty} \frac{x^i}{\Gamma(\phi i + \mu)}$, where $\phi, \mu \in \mathbb{R}$.

Theorem 1 [17] Let $\alpha > 0$, $\alpha \in (n-1, n)$, $n \in \mathbb{N}$. The function $f(t)$ is considered to be continuously differentiable over (t_0, ∞) up to order $n-1$ so that there exists an n^{th} derivative of $f(t)$ having exponential order. When ${}_{t_0}^{C}D_t^{\alpha} f(t)$ is piecewise continuous on (t_0, ∞), then $L\left[{}_{t_0}^{C}D_t^{\alpha} f(t)\right] = s^{\alpha} F(s) - \sum_{i=0}^{n-1} s^{\alpha-i-1} f^i(t_0)$, in which $F(s) = L[f(t)]$.

Theorem 2 [18] For system $D_t^{\alpha} x(t) = f(t, x(t))$, $x(0) = x_0$, where the function $f(t, x(t)) : \mathbb{R}^+ \times \mathbb{R}^n \to \mathbb{R}^n$ and $\alpha \in 0, 1$, when the absolute value of the function $\arg(\lambda_i)$ is greater than $\frac{\alpha\pi}{2}$, the system's equilibrium point is locally asymptotically stable, with λ_i denoting its latent values.

3. The distinctiveness and boundedness

Theorem 3 System (3) admits only one solution.

Proof. The presence and distinctive nature of the solution for the framework (3) within the domain $[0, \tau] \times \Upsilon$ is explored, in which $\Upsilon = \{(X, Y) \in \Re^2 : 0 \leq X, Y \leq P\}$.

Assume $G = (X, Y)$, $\bar{G} = (\bar{X}, \bar{Y})$, $F(G) = (F_1(G), F_2(G))$ and

$$F_1(G) = X(1-X) - \frac{\tilde{a}XY}{1+\tilde{b}X} - \tilde{q}_1 X - \tilde{d}_1 X^2,$$

$$F_2(G) = \tilde{s}Y(1-Y) + \frac{\tilde{c}\tilde{a}XY}{1+\tilde{b}X} - \tilde{q}_2 Y - \tilde{d}_2 Y. \tag{4}$$

For any $G, \bar{G} \in \Upsilon$, it follows from (4) that

$$\begin{aligned}
&\|F(G) - F(\bar{G})\| \\
&= \left\|F_1(G) - F_1(\bar{G})\right\| + \left\|F_2(G) - F_2(\bar{G})\right\| \\
&= \left|X(1-X) - \frac{\tilde{a}XY}{1+\tilde{b}X} - \tilde{q}_1 X - \tilde{d}_1 X^2 - \bar{X}(1-\bar{X}) + \frac{\tilde{a}\bar{X}\bar{Y}}{1+\tilde{b}\bar{X}} + \tilde{q}_1 \bar{X} + \tilde{d}_1 \bar{X}^2\right|
\end{aligned}$$

$$+\left|\tilde{s}Y(1-Y)+\frac{\tilde{c}\tilde{a}XY}{1+\tilde{b}X}-\tilde{q}_2Y-\tilde{d}_2Y-\tilde{s}\bar{Y}(1-\bar{Y})-\frac{\tilde{c}\tilde{a}\bar{X}\bar{Y}}{1+\tilde{b}\bar{X}}+\tilde{q}_2\bar{Y}+\tilde{d}_2\bar{Y}\right|$$

$$\leq \left(1+2P+2P\tilde{d}_1+\tilde{q}_1+\frac{P\tilde{a}(1+\tilde{c})}{(1+\tilde{b}P)^2}\right)|X-\bar{X}|$$

$$+\left(\tilde{s}+2P\tilde{s}+\tilde{q}_2+\tilde{d}_2+\frac{P\tilde{a}(1+\tilde{c})}{1+\tilde{b}P}\right)|Y-\bar{Y}|$$

$$\leq L\|G-\bar{G}\|,$$

where

$$L=\max\left\{1+2P+2P\widetilde{d}_1+\widetilde{q}_1+\frac{P\widetilde{a}(1+\widetilde{c})}{\left(1+\widetilde{b}P\right)^2},\ \widetilde{s}+2P\widetilde{s}+\widetilde{q}_2+\widetilde{d}_2+\frac{P\widetilde{a}(1+\widetilde{c})}{1+\widetilde{b}P}\right\}.$$

As stated in Lemma 2 of [19], $F(G)$ adheres to the local Lipschitz criteria. Consequently, framework (3) offers a distinct solution in Υ.

Theorem 4 System (3) has a solution that is bounded, therefore

$$\chi=\left\{(X,Y)\in\mathbb{R}^2:0<X+\frac{1}{\widetilde{c}}Y<\frac{(1-\widetilde{q}_1+\sigma)^2}{4\left(1+\widetilde{d}_1\right)}\right\}$$

is absolutely unaltered over the system.

Proof. Let $F(T)=X(T)+\frac{1}{\widetilde{c}}Y(T)$, then one has

$$D_\tau^\alpha F(T)+\sigma F(T)=X(1-X)-\frac{\tilde{a}XY}{1+\tilde{b}X}-\tilde{q}_1X-\tilde{d}_1X^2$$

$$+\frac{1}{\tilde{c}}\left(\tilde{s}Y(1-Y)+\frac{\tilde{c}\tilde{a}XY}{1+\tilde{b}X}-\tilde{q}_2Y-\tilde{d}_2Y\right)+\sigma\left(X+\frac{1}{\tilde{c}}Y\right),$$

$$F(T)+\sigma F(T)\leq-\left(1+\widetilde{d}_1\right)\left(X-\frac{(1-\widetilde{q}_1+\sigma)}{2\left(1+\widetilde{d}_1\right)}\right)^2+\frac{(1-\widetilde{q}_1+\sigma)^2}{4\left(1+\widetilde{d}_1\right)}. \tag{5}$$

Let $u=\dfrac{(1-\widetilde{q}_1+\sigma)^2}{4\left(1+\widetilde{d}_1\right)}$. It is possible to rewrite equation (5) as

$$D_{\tau}^{\alpha}F(T)+\sigma F(T)\leq u. \tag{6}$$

Take either side through the Laplace transform,

$$s^{\alpha}F(s)-s^{\alpha-1}f(0)+\sigma F(s)\leq \frac{u}{s},$$

$$F(s)\leq \frac{s^{\alpha}f(0)+u}{s\left(s^{\alpha}+\sigma\right)},$$

$$F(s)\leq \frac{s^{\alpha-1}f(0)}{\left(s^{\alpha}+\sigma\right)}+\frac{u}{s\left(s^{\alpha}+\sigma\right)}. \tag{7}$$

Make use of Laplace inversion

$$f(t)\leq f(0)L^{-1}\left[\frac{s^{\alpha-1}}{s^{\alpha}+\sigma}\right]+uL^{-1}\left[\frac{s^{\alpha-(\alpha+1)}}{s^{\alpha}+\sigma}\right]. \tag{8}$$

Another way to express equation (8) is as

$$f(t)\leq f(0)E_{\alpha,\,1}\left(-\sigma t^{\alpha}\right)+ut^{\alpha}E_{\alpha,\,\alpha+1}\left(-\sigma t^{\alpha}\right). \tag{9}$$

One can ascertain that

$$E_{\alpha,\,\beta}(x)=xE_{\alpha,\,\alpha+\beta}(x)+\frac{1}{\Gamma(\beta)}. \tag{10}$$

If we set $\beta=1$, $x=-\sigma t^{\alpha}$, then the result of equation (10) is

$$E_{\alpha,\,1}\left(-\sigma t^{\alpha}\right)=-\sigma t^{\alpha}E_{\alpha,\,\alpha+1}\left(-\sigma t^{\alpha}\right)+1, \tag{11}$$

$$t^{\alpha}E_{\alpha,\,\alpha+1}\left(-\sigma t^{\alpha}\right)=-\frac{1}{\sigma}\left(E_{\alpha,\,1}\left(-\sigma t^{\alpha}\right)-1\right). \tag{12}$$

The subsequent outcome arises from substituting expression (12) into (9),

$$f(t)\leq f(0)E_{\alpha,\,1}\left(-\sigma t^{\alpha}\right)-\frac{u}{\sigma}\left(E_{\alpha,\,1}\left(-\sigma t^{\alpha}\right)-1\right),$$

$$f(t) \leq \frac{u}{\sigma} + \left(f(0) - \frac{u}{\sigma}\right) E_{\alpha,1}\left(-\sigma t^{\alpha}\right). \tag{13}$$

Based on the Mittag-Leffler function's properties, $E_{\alpha,1}\left(-\sigma t^{\alpha}\right) > 0$, on every $t \geq 0$. The result of (13) indicates that once the initial value meets the condition $f(0) \leq \frac{u}{\sigma}$, subsequently any value $t \geq 0$, $f(t) \leq \frac{u}{\sigma}$. Based on the non-negativity of the framework (3), for every $t \geq 0$, $f(t) \geq 0$, χ constitutes a positive unaltered set concerning the framework (3).

Since the Mittag-Leffler function has the property that $\underset{t\to\infty}{lt} E_{\alpha,1}\left(-\sigma t^{\alpha}\right) = 0$, if $f(0) > \frac{u}{\sigma}$ in the initial stage, hence $\underset{t\to\infty}{lt} f(t) \leq \frac{u}{\sigma} + \left(f(0) - \frac{u}{\sigma}\right) \underset{t\to\infty}{lt} E_{\alpha,1}\left(-\sigma t^{\alpha}\right) = \frac{u}{\sigma}$. As a result, system (3) has a bounded solution.

4. Steady states and stability analysis

The dynamical system (3) may stabilise in the manner described here: $E_0 = (0, 0)$, $E_1 = \left(\frac{1-\widetilde{q}_1}{1+\widetilde{d}_1}, 0\right)$, for $X = \frac{1-\widetilde{q}_1}{1+\widetilde{d}_1}$, it is essential that $1-\widetilde{q}_1 > 0$, which guarantees a positive steady state for prey alone, and $E^* = (X^*, Y^*)$, in which $Y^* = \frac{\left(1-X^*-\widetilde{q}_1-\widetilde{d}_1X^*\right)\left(1+\widetilde{b}X^*\right)}{\widetilde{a}}$, and X^*can be obtained from

$$A_0 X^{*3} + A_1 X^{*2} + A_2 X^* + A_3 = 0, \tag{14}$$

in which

$$A_0 = \widetilde{s}\widetilde{b}^2,$$

$$A_1 = \widetilde{s}\widetilde{b}\left(2 - \widetilde{b} + \widetilde{q}_1\widetilde{b} + 2\widetilde{d}_1 + \widetilde{d}_1\widetilde{b}\right),$$

$$A_2 = \left(\widetilde{a}\widetilde{s}\widetilde{b} - 2\widetilde{s}\widetilde{b} + \widetilde{s} + 2\widetilde{s}\widetilde{q}_1\widetilde{b} + \widetilde{s}\widetilde{d}_1 - \widetilde{a}\widetilde{q}_2\widetilde{b} - \widetilde{a}\widetilde{d}_2\widetilde{b} + \widetilde{c}\widetilde{a}^2\right),$$

$$A_3 = \widetilde{a}\widetilde{s} - \widetilde{s} + \widetilde{s}\widetilde{q}_1 - \widetilde{a}\widetilde{q}_2 - \widetilde{a}\widetilde{d}_2.$$

In order to analyse the local permanency of the framework (3), it is essential for determining the community matrix at the fixed points that have been found below.

$$J = \begin{pmatrix} (1-2X) - \dfrac{\widetilde{a}Y}{\left(1+\widetilde{b}X\right)^2} - \widetilde{q}_1 - 2\widetilde{d}_1X & -\dfrac{\widetilde{a}X}{1+\widetilde{b}X} \\ \dfrac{\widetilde{c}\widetilde{a}Y}{\left(1+\widetilde{b}X\right)^2} & \widetilde{s}(1-2Y) + \dfrac{\widetilde{c}\widetilde{a}X}{1+\widetilde{b}X} - \widetilde{q}_2 - \widetilde{d}_2 \end{pmatrix}.$$

Theorem 5 The framework (3) confirms local asymptotic resilience near the trivial equilibrium point $E_0 = (0, 0)$, if $\widetilde{q}_1 > 1$ and $\widetilde{s} < \widetilde{q}_2 + \widetilde{d}_2$.

Proof. Finding the community matrix at E_0 is possible by $J(E_0) = \begin{pmatrix} 1-\widetilde{q}_1 & 0 \\ 0 & \widetilde{s}-\widetilde{q}_2-\widetilde{d}_2 \end{pmatrix}$. The eigenvalues are given by $\lambda_1 = 1-\widetilde{q}_1$, $\lambda_2 = \widetilde{s} - \left(\widetilde{q}_2 + \widetilde{d}_2\right)$. By using Theorem 2, we can conclude that it is locally asymptotically stable if $\widetilde{q}_1 > 1$ and $\widetilde{s} < \widetilde{q}_2 + \widetilde{d}_2$. A saddle point having stable manifold along the X-axis and unstable manifold along the Y-axis if and only if $\widetilde{q}_1 < 1$ (> 1), $\widetilde{s} > (<)$ $\widetilde{q}_2 + \widetilde{d}_2$. It is unstable for $\widetilde{q}_1 < 1$ and $\widetilde{s} > \widetilde{q}_2 + \widetilde{d}_2$.

Theorem 6 The framework (3) exhibits local asymptotic resilience near the equilibrium point $E_1 = \left(\frac{1-\widetilde{q}_1}{1+\widetilde{d}_1}, 0\right)$, if $\widetilde{s} < \widetilde{q}_2 + \widetilde{d}_2$ and $\left[\left(1+\widetilde{d}_1\right) + \widetilde{b}(1-\widetilde{q}_1)\right] < \frac{\widetilde{c}\widetilde{a}(1-\widetilde{q}_1)}{\left[\widetilde{s} - \left(\widetilde{q}_2 + \widetilde{d}_2\right)\right]}$.

Proof. For E_1, the community matrix as follows

$$J(E_1) = \begin{pmatrix} (1-2X) - \widetilde{q}_1 - 2\widetilde{d}_1 X & -\frac{\widetilde{a}X}{1+\widetilde{b}X} \\ 0 & \widetilde{s} + \frac{\widetilde{c}\widetilde{a}X}{1+\widetilde{b}X} - \widetilde{q}_2 - \widetilde{d}_2 \end{pmatrix}.$$

The eigenvalues are given by $\lambda_1 = (1-2X) - \widetilde{q}_1 - 2\widetilde{d}_1 X$ and $\lambda_2 = \widetilde{s} + \frac{\widetilde{c}\widetilde{a}X}{1+\widetilde{b}X} - \widetilde{q}_2 - \widetilde{d}_2$. At the equilibrium point the eigenvalue $\lambda_1 < 0$ always and $\lambda_2 < 0$ for $\widetilde{s} < \widetilde{q}_2 + \widetilde{d}_2$ and $\left[\left(1+\widetilde{d}_1\right) + \widetilde{b}(1-\widetilde{q}_1)\right] < \frac{\widetilde{c}\widetilde{a}(1-\widetilde{q}_1)}{\left[\widetilde{s} - \left(\widetilde{q}_2 + \widetilde{d}_2\right)\right]}$. By using Theorem 2, one can deduce that it exhibits local asymptotic stability. Alternatively, it constitutes a saddle point if $\lambda_2 > 0$ for $\widetilde{s} > \widetilde{q}_2 + \widetilde{d}_2$.

Theorem 7 The framework (3) exhibits local asymptotic stability around the equilibrium point $E^* = (X^*, Y^*)$ provided one of the subsequent criteria are met.

(i) $Trace\left(J(E^*)\right) \leq 0$,

(ii) $Trace\left(J(E^*)\right) > 0$, $Trace^2\left(J(E^*)\right) - 4\left|J(E^*)\right| < 0$ and

$$sqrt\left(\left|Trace^2\left(J(E^*)\right) - 4\left|J(E^*)\right|\right|\right) > Trace\left(J(E^*)\right)\tan\left(\frac{\alpha\pi}{2}\right).$$

Proof. For E^*, the community matrix as follows

$$J(E^*) = \begin{pmatrix} -X\left(1+\widetilde{d}_1\right) + \frac{\widetilde{a}\widetilde{b}XY}{\left(1+\widetilde{b}X\right)^2} & -\frac{\widetilde{a}X}{1+\widetilde{b}X} \\ \frac{\widetilde{c}\widetilde{a}Y}{\left(1+\widetilde{b}X\right)^2} & -\widetilde{s}Y \end{pmatrix}.$$

For above Jacobian matrix

$$Trace\left(J\left(E^*\right)\right) = -X\left(1+\widetilde{d_1}\right) + \frac{\widetilde{a}\widetilde{b}XY}{\left(1+\widetilde{b}X\right)^2} - \widetilde{s}Y$$

and

$$\det\left(J\left(E^*\right)\right) = XY\widetilde{s}\left(1+\widetilde{d_1}\right) + \frac{\widetilde{a}XY\left[\widetilde{c}\widetilde{a} - \widetilde{s}\widetilde{b}Y\left(1+\widetilde{b}X\right)\right]}{\left(1+\widetilde{b}X\right)^3}.$$

(i) When sum of latent values of $\left(J\left(E^*\right)\right) \leq 0$ then there are three scenarios that we need to take into consideration.

In the scenario a), where sum of latent values of $\left(J\left(E^*\right)\right) = 0$, we find that $\left|\arg\left(\lambda_i\right)\right| = \frac{\alpha\pi}{2}$, $i = 1, 2$ indicating that $E^*$is locally asymptotically stable.

In the scenario b), where sum of latent values of $\left(J\left(E^*\right)\right) < 0$ along with $Trace^2\left(J\left(E^*\right)\right) - 4\left|J\left(E^*\right)\right| \geq 0$, subsequently each latent value is not positive together with $\left|\arg\left(\lambda_i\right)\right| = \pi$, $i = 1, 2$. Therefore, E^* exhibits local asymptotic stability.

In the scenario c), where sum of latent values of $\left(J\left(E^*\right)\right) < 0$ as well as $Trace^2\left(J\left(E^*\right)\right) - 4\left|J\left(E^*\right)\right| < 0$, subsequently the two latent values are complex conjugates with a negative real part along with $\left|\arg\left(\lambda_i\right)\right| > \frac{\alpha\pi}{2}$, $i = 1, 2$. Consequently, E^* exhibits local asymptotic stability for any α.

(ii) If $Trace(J(E^*)) > 0$, $Trace^2(J(E^*)) - 4\det(J(E^*)) < 0$ and $sqrt\left(\left|Trace^2(J(E^*)) - 4\det(J(E^*))\right|\right) > Trace\left(J(E^*)\right)\tan\left(\frac{\alpha\pi}{2}\right)$ then we obtain $Img\left(\lambda_1\right) = -Img\left(\lambda_2\right) = 4\det\left(J\left(E^*\right)\right) - Trace^2\left(J\left(E^*\right)\right)$ and $Re\left(\lambda_i\right) =$ sum of latent values of $J\left(E^*\right) > 0$, $i = 1, 2$.

Given these, it is easy to see that $\left|Img\left(\lambda_i\right)\right| > \tan\left(\frac{\alpha\pi}{2}\right)\left(Re(\lambda_i)\right)$, $i = 1, 2$. Therefore, it can be shown that E^* is locally asymptotically resilient given the condition that $\left|\arg\left(\lambda_i\right)\right| > \frac{\alpha\pi}{2}$, $i = 1, 2$.

5. Hopf bifurcation

In the presence of two complementary latent values of the linearised system's community matrix, the system undergoes Hopf bifurcation close to any coexistence equilibrium. Periodic solutions are either generated or destroyed in this situation. When the bifurcation parameter crosses the critical value, the state of equilibrium transitions via a stable condition to an unstable one, or vice versa.

According to the earlier findings, the model system's resilience is significantly impacted through the derivative order. The bifurcation parameter of the framework (3) is possible to designated as order (α). Hopf bifurcation conditions in non-integer order systems are, with a few exceptions, very analogous to those in integer order frameworks. Take into account the fractional order scheme below.

$$_{t_0}^{C}D_t^{\alpha}x = f(\mu, x),$$

where $\alpha \in (0, 1)$, $x \in \mathbb{R}^2$.

Assuming E is a system equilibrium point, a Hopf bifurcation occurs at μ^* of μ when all of these criteria are satisfied [20]:

(i) The system's Jacobian matrix at the equilibrium includes two complex conjugate eigenvalues, $\lambda_{1,2}^k = \varphi_k \pm i\psi_k$ which turn entirely imaginary at $\mu = \mu^*$.

(ii) $\vartheta_k(\alpha, \mu^*) = 0$, $k = 1, 2$.

(iii) $\frac{\partial \vartheta_k}{\partial \mu}|_{\mu=\mu^*} \neq 0$, where $\vartheta_k(\alpha, \mu) = \frac{\alpha\pi}{2} - \min_{i=1,2} |\arg(\lambda_i(\mu))|$.

Upon selecting α as the transition parameter, the non-integer order framework experiences a Hopf bifurcation closest to the equilibrium point at the crucial value $\alpha = \alpha^*$.

6. Numerical simulations

The fractional order systems were solved by Diethelm [21, 22] using the Adams-Bashforth-Moulton approach, which relies on the predictor-corrector methodology. The following simulations were conducted using MATLAB R2024a.

For this study, we used three distinct system (3) scenarios, each with its own set of parameters, including order of differentiation (α), toxicity effect $(\widetilde{d}_1, \widetilde{d}_2)$, and harvesting effect $(\widetilde{q}_1, \widetilde{q}_2)$. As demonstrated in Figure 1 and Figure 2, one can alter the stability of the coexistence equilibrium point by modifying the order of the derivatives (α), while keeping all other parametric values constant. When (α) is close to 0.92, the periodic solutions in system (3) emerge, and at the same time, the Hopf bifurcation system occurs.

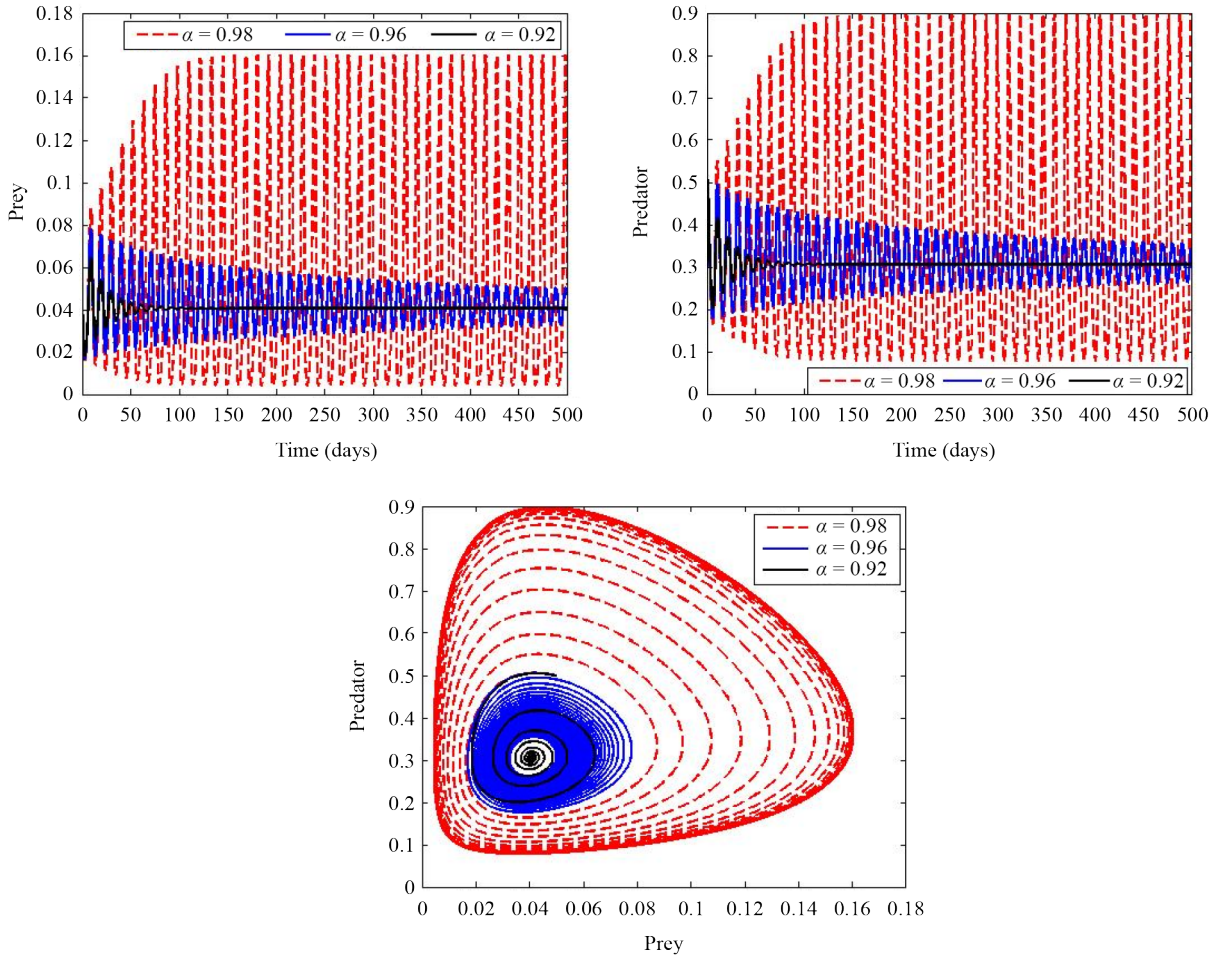


Figure 1. Time series and phase portrait for framework (3) are associated with α values of 0.92, 0.96, and 0.98, other parameter values are $\widetilde{a} = 3.564$, $\widetilde{b} = 5.015$, $\widetilde{q}_1 = 0.0381$, $\widetilde{d}_1 = 0.381$, $\widetilde{s} = 0.065$, $\widetilde{c} = 4.452$, $\widetilde{q}_2 = 0.000295$, $\widetilde{d}_2 = 0.58$

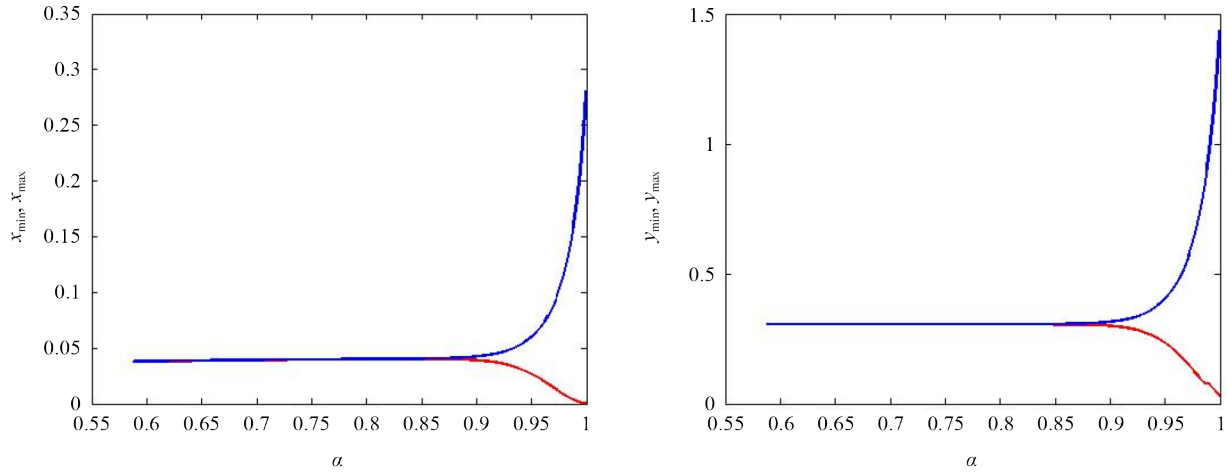


Figure 2. Using α to indicate the bifurcation variable, the system (3) bifurcation diagram shows that Hopf bifurcation takes at $\alpha = 0.92$

Our numerical simulations of model (3) have shown that the model's qualitative properties can be changed by varying the intensities of harmful compounds produced by the two species. When a species goes extinct, toxicity could be the cause. As can be seen from the numerical simulations, Figure 3 illustrates how a slow increase in $\widetilde{d_1}$ results in a decline in the first species' population and a decline in the other species' population as a consequence of less prey being available. Similarly, Figure 4 shows that a little increase in $\widetilde{d_2}$ results in a drop in second species and an increase in first species. Additionally, Figures 5 and 6 illustrate Hopf bifurcation in relation to the impact of toxicity parameters $\widetilde{d_1}$ and $\widetilde{d_2}$. Based on the results, it seems the scenario for the system's resilience could change based on the intensity of the toxin release by the two species.

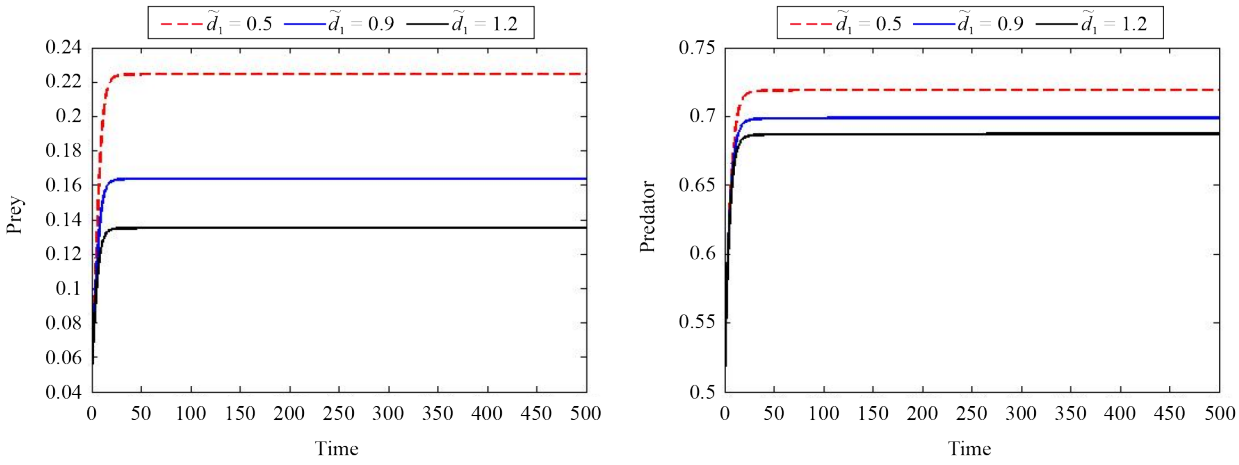


Figure 3. Multiple portraits for system (3) when $\widetilde{d_2} = 0.2$ and $\widetilde{d_1} = 0.5, 0.9, 1.2$, other parametric values are $\widetilde{a} = 0.6138$, $\widetilde{b} = 3.6074$, $\widetilde{q_1} = 0.4191$, $\widetilde{s} = 0.5$, $\widetilde{c} = 0.78652$, $\widetilde{q_2} = 2.95E-4$

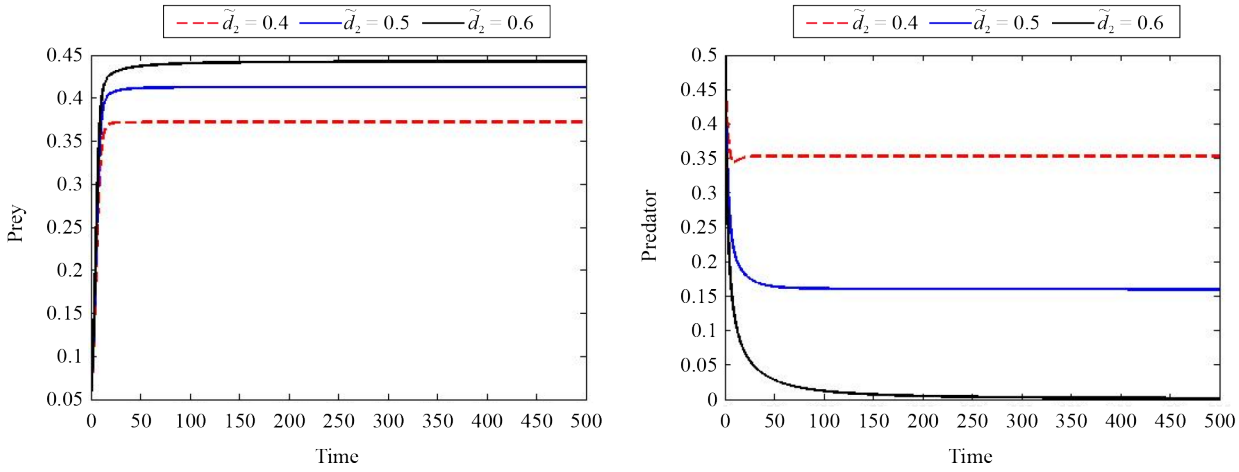


Figure 4. Multiple portraits for system (3) when $\widetilde{d}_1 = 0.312$ and $\widetilde{d}_2 = 0.4, 0.5, 0.6$, other parametric values are same as in Figure 3

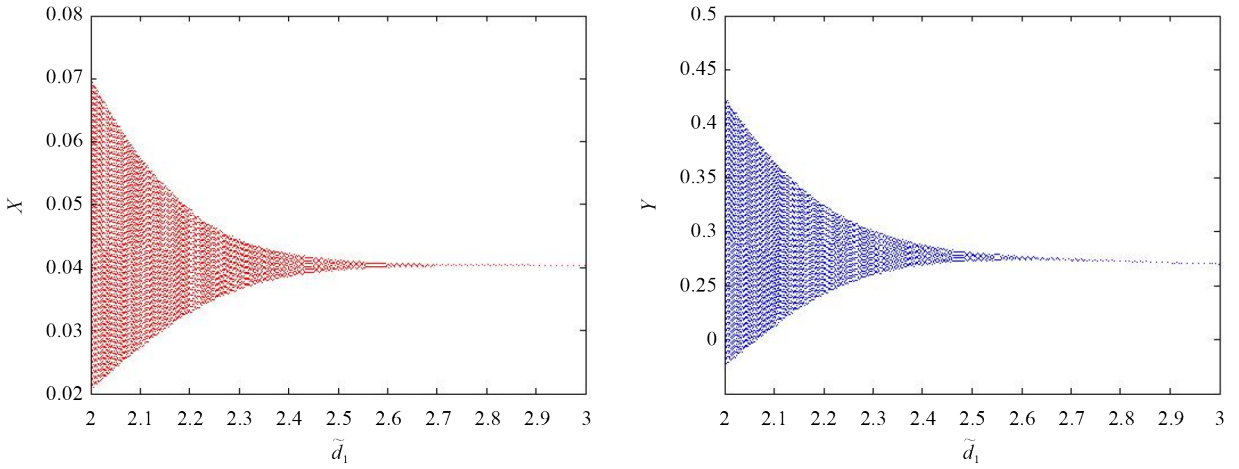


Figure 5. System (3)'s bifurcation diagram with respect to $\widetilde{d}_1$, all other parameters remain the same that are illustrated in Figure 1 with $\alpha = 1$

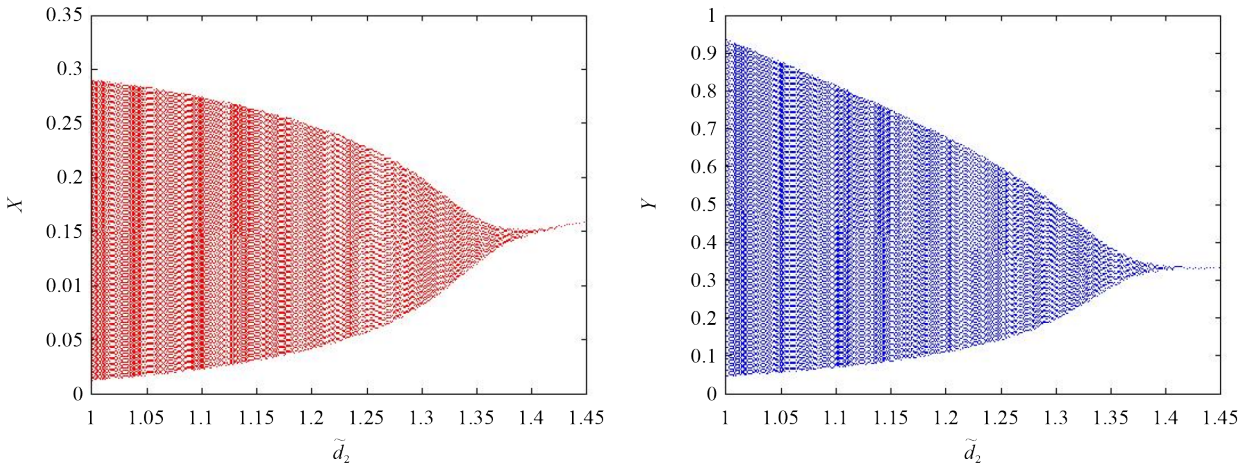


Figure 6. System (3)'s bifurcation diagram with respect to $\widetilde{d}_2$, all other parameters remain the same that are illustrated in Figure 1 with $\alpha = 1$

We can now observe that when $\widetilde{q}_1$ is increased for a fixed $\widetilde{q}_2$, the prey population declines, which in turn causes the predator population to decline because there is less prey available. Furthermore, as Figure 7 illustrates, an excess of $\widetilde{q}_1$ may cause the system to become unstable, resulting in the extinction of both prey and predators. In the same way, when $\widetilde{q}_2$ is increased for a fixed $\widetilde{q}_1$, the predator population declines and the prey population rises as a result of less predation pressure. Additionally, as illustrated in Figure 8, an excess of $\widetilde{q}_2$ may cause prey overpopulation and predator extinction, destabilising the system. Furthermore, Hopf bifurcation in connection to the influence of harvesting parameters $\widetilde{q}_1$ and $\widetilde{q}_2$ is depicted in Figures 9 and 10. Both populations stabilise above a critical value of $\widetilde{q}_1$, suggesting that excessive prey harvesting removes the oscillatory dynamics between predators and prey. In a similar way a critical $\widetilde{q}_2$ is probably where a Hopf bifurcation is seen. While larger values stabilise the system, smaller values permit oscillatory behaviour.

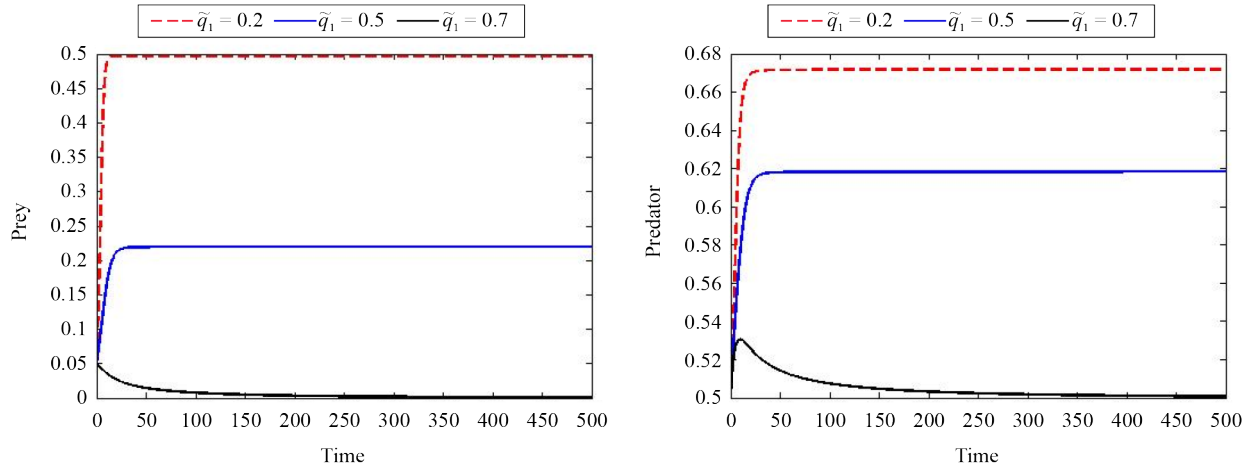


Figure 7. Multiple portraits for system (3) when $\widetilde{q}_2 = 0.05$ and $\widetilde{q}_1 = 0.2, 0.5, 0.7$, other parameters are $\widetilde{a} = 0.6138$, $\widetilde{b} = 3.6074$, $\widetilde{d}_1 = 0.312$, $\widetilde{s} = 0.5$, $\widetilde{c} = 0.78652$, $\widetilde{d}_2 = 0.2$

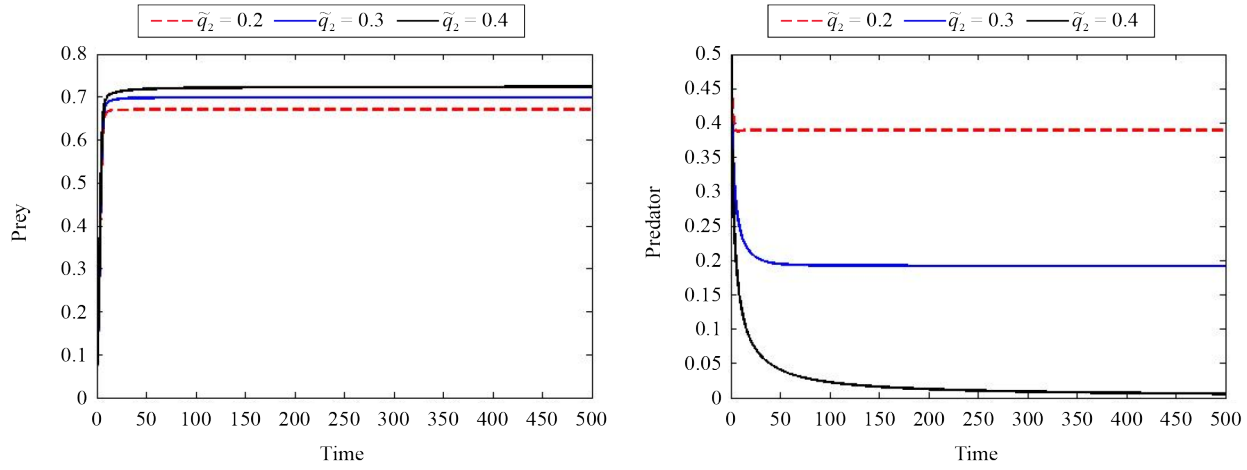


Figure 8. Multiple portraits for system (3) when $\widetilde{q}_1 = 0.05$ and $\widetilde{q}_2 = 0.2, 0.3, 0.4$, other parametric values are same as in Figure 7

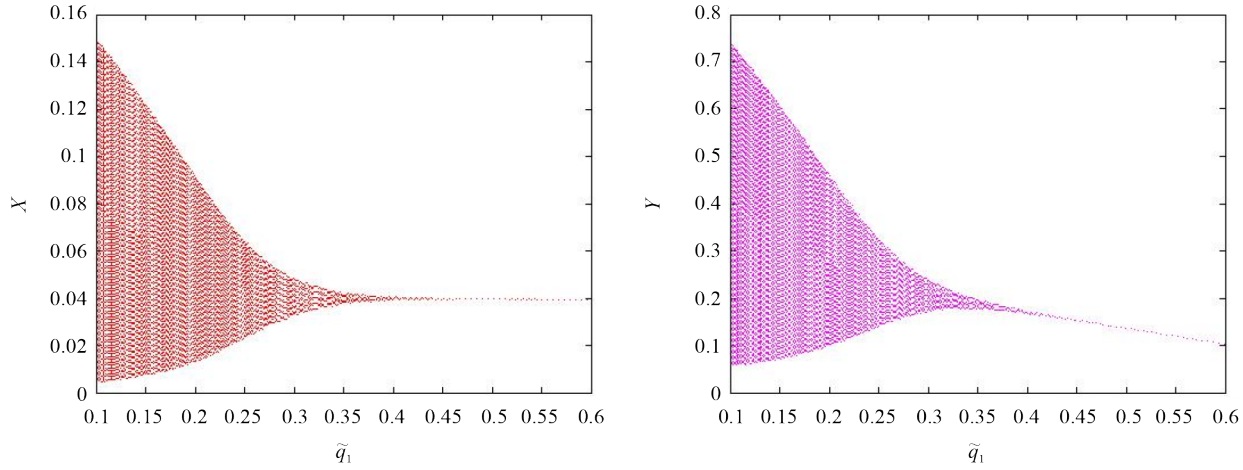


Figure 9. System (3)'s bifurcation diagram with respect to $\widetilde{q}_1$, all other parameters are identical to those in Figure 1 with $\alpha = 1$

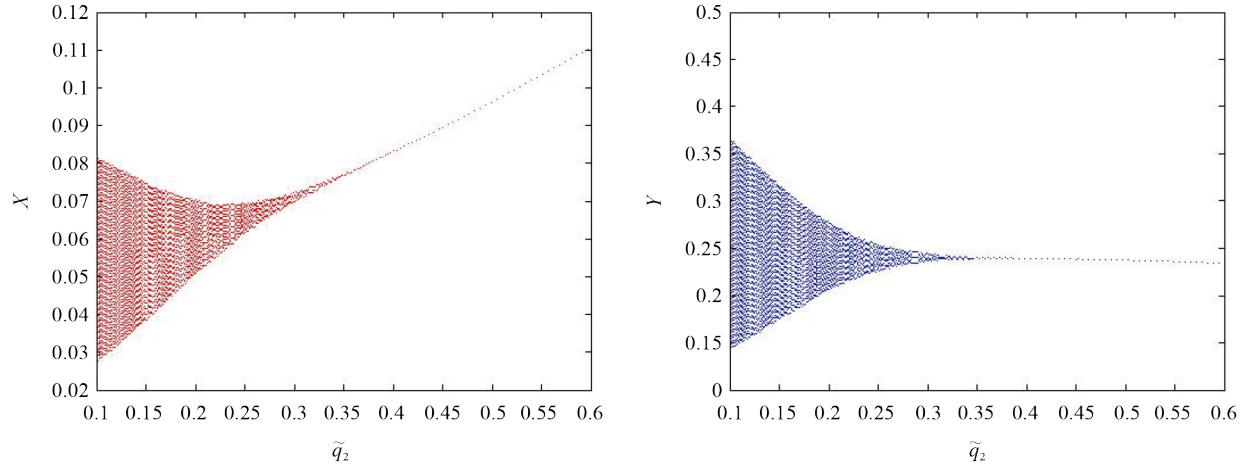


Figure 10. The bifurcation diagram of the system (3) about $\widetilde{q}_2$ other parametric values are same as in Figure 1 with $\alpha = 1$

7. Neural networking analysis

The provided MATLAB code leverages a feedforward neural network to recreate the dynamics of the system and incorporates a classical prey-predator model that includes harvesting effects for both species. Growth rates, sustaining capacities, predation level, handling time, harvesting levels, and self-limitation terms are among the model components that have been carefully selected to reflect actual interactions involving prey and predator populations. By considering the prey class "y" for the neural network analysis. Numerical data taken from the numerical method used and the datasets are distributed for training = 375, validation = 75, and testing = 75. For instance, the predator growth rate is slightly smaller at 0.7, revealing a slower increase in comparison to prey, while the prey growth rate is set at 0.8, showing a relatively quick growth process. Prey and predators have carrying capacity of 10 and 8, thereby, which limit population levels and cause expansion of logistics behaviour. With a dealing time factor of 0.4 and a predation rate of 0.5, the predation term reveals a Holling type II functional response which catches the saturation effect at large prey populations. For both species, harvesting terms with indices of 0.02 and harvesting attempts of 0.1 are considered, denoting outside factors like fishing or human activity. In addition, the model is stabilised and unlimited growth is impeded by self-limitation and natural death

rates, which are 0.03 for prey and 0.04 for predators. The Figure 11 showing neural network procedure. For further details of neural networking one can study [23–27].

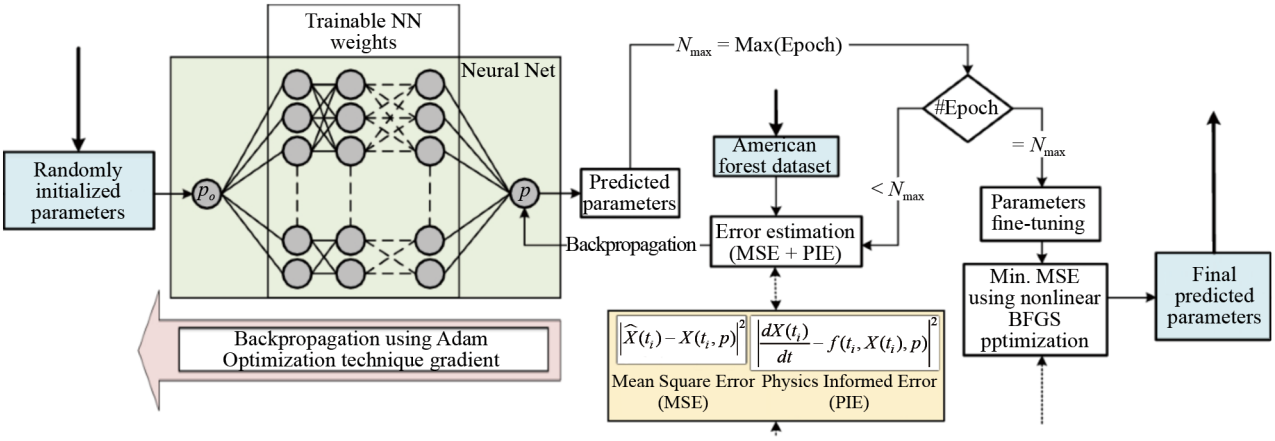


Figure 11. Neural networking analysis of Eq. (2) pre-predator model

The numerical simulation is employed for effectively determining the prey and predator communities over a 50-unit time span using the classical fourth-fifth order Runge-Kutta approach. There is an inherent disproportion between the two species in the starting scenario with 2 prey and 1 predator. A feedforward neural network is developed using the time-series data donated by the corresponding numerical solution for both species.

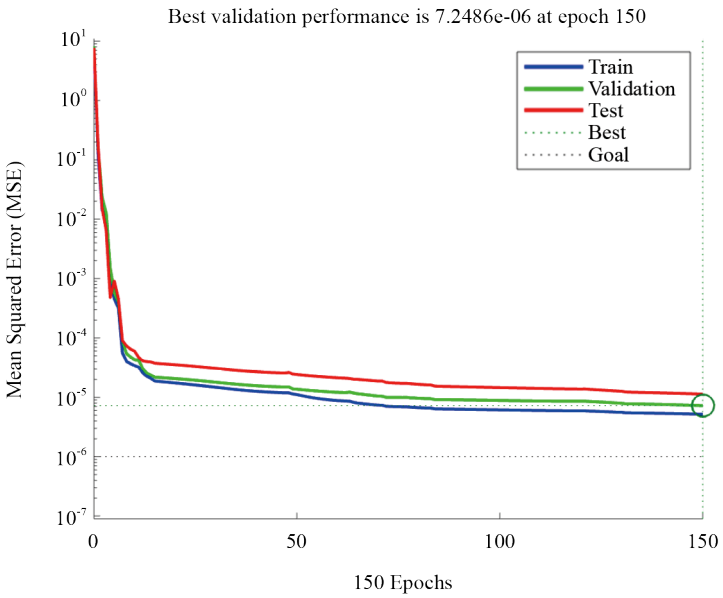


Figure 12. Best validation of Eq. (2) pre-predator model

Prediction, control, and evaluation of sensitivity can all benefit from the neural network's smooth and continuous illustration, from which it learns by estimating the populations at any given time and incorporating their fundamental dynamics. For the aim of approximation, a feedforward neural network is implemented, which has one hidden layer and ten neurones.

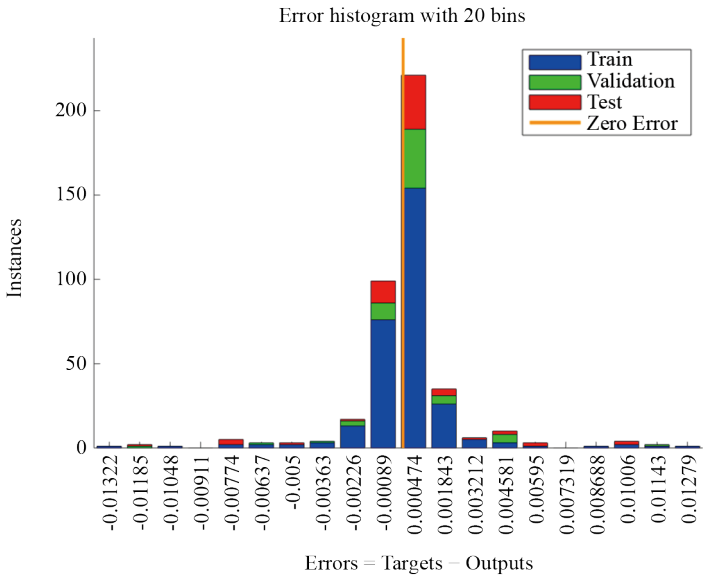


Figure 13. Error histogram of pre-predator model

When training, the network is subjected to the Levenberg-Marquardt technique, which merges the benefits of downward gradient descent and the Gauss-Newton methodology for enabling rapid convergence for challenges of small to medium scale. To prevent overfitting, the training method is set up to run for 150 epochs, which is enough iterations for guaranteed convergence. In order to train the network to minimise the mean squared error over its outputs and the numerical outcome, the network constantly adjusts its weights. After the training completes, the network obtains a performance of about 5.19×10^{-6}, suggesting that the calculated populations are quite near to the numerical result. The great degree of accuracy of the neural network estimation is shown by this low performance metric. Providing a measure of how sensitive the performance indicator is to the network weights at the last step, the gradient value is recorded at 0.000326. Considering the network has found its near-optimal configuration, a modest gradient demonstrates that modifying the weights has minimal impact on the reduction of error. The Levenberg-Marquardt technique's damping factor, mu, governs the step size when adjusting the weights and is set to 1.0×10^{7}. Gradual contraction provides fast convergence as the network approaching the perfect outcome, while a large mu initially stabilises the learning and eliminates divergence. It is common practice for assessing the trained neural network's forecasts to the initial numerical estimate after training. The network accurately demonstrates the delicate harvesting and self-limitation behaviours as well as the rhythmic prey-predator connections.

The plots show that the numerical and neural network results are very congruent, which indicates that the approximation is accurate. The Figure 12, Best validation of Eq. (2) pre-predator model, Figure 13, Error Histogram of pre-predator model and Figure 14, Performance of pre-predator model. In order to accomplish such a high level of accuracy, it is essential for using 150 epochs, carefully manage the performance objective, and establish the network design correctly. When employed together, computational modelling and neural network approximation form a solid foundation for describing intricate ecological interactions, permitting rapid scenario-specific response prediction.

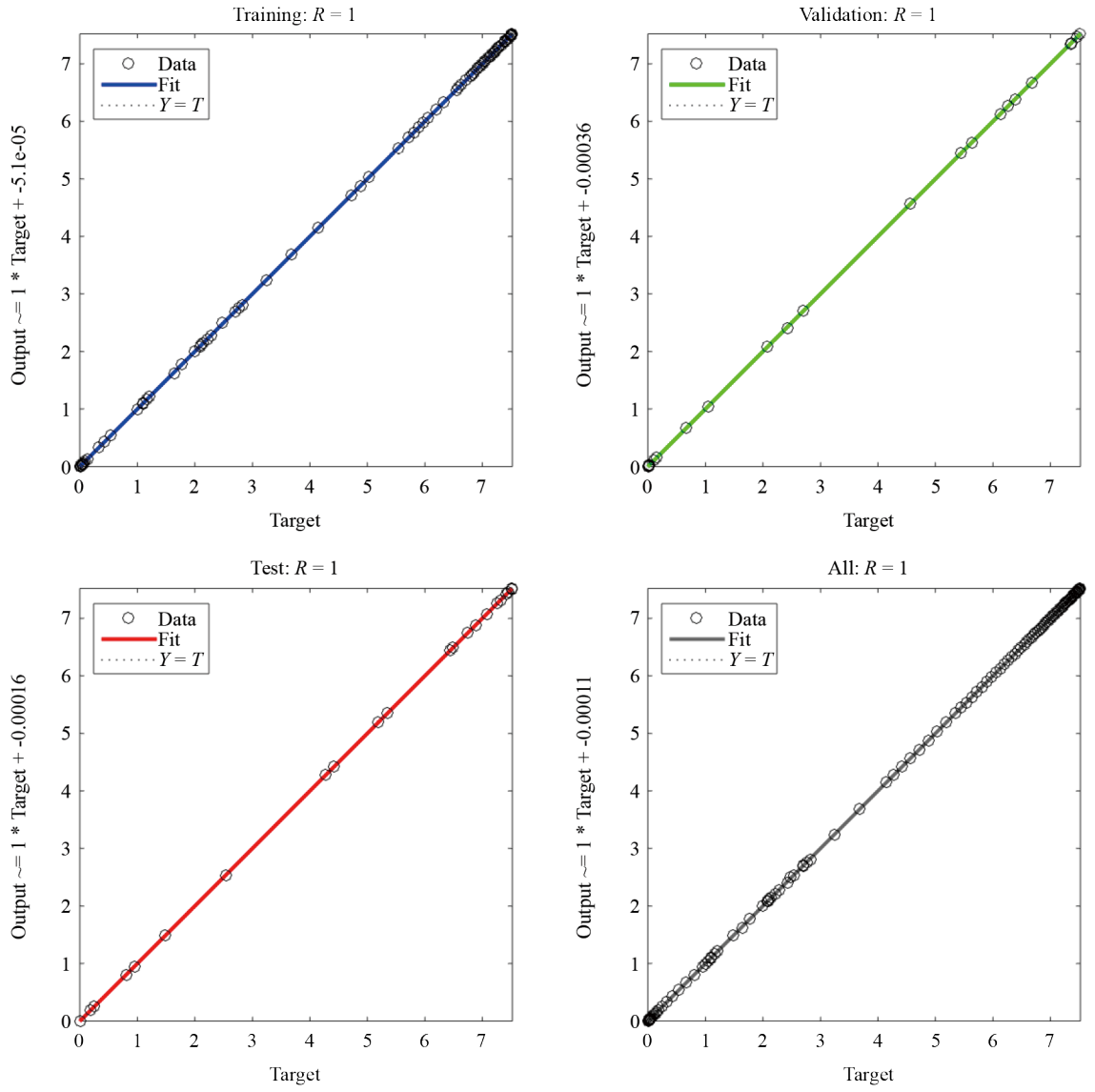


Figure 14. Performance of pre-predator model

8. Conclusions

Exploring the effects of toxicity and harvesting on the evolutionary mechanisms of a non-integer order pair of species system is the main emphasis of this paper. System (3) has been examined for its distinctiveness and boundedness. The equilibria have been shown to be locally stable. Numerical simulations of model (3) presented in Figure 1 indicate that fractional order significantly influences population dynamics. Changing the order of the derivatives, while holding all other parametric values constant, changes the stability condition of the equilibrium point. Specifically, a Hopf bifurcation for the framework (3) has been identified at a particular derivative order. For the numerical method validation neural network analysis used for error analysis.

Additionally, we can observe from simulations that the predator population is indirectly impacted by rising prey toxicity $\widetilde{d_1}$, although the toxicity term $\widetilde{d_2}$ remains constant. Predator famine, decreased reproduction, and ultimately population collapse can result from lower prey abundance, as Figures 3 and 4 illustrate. Furthermore, Hopf bifurcation is depicted in Figures 5 and 6 along with the influence of toxicity factors $\widetilde{d_1}$ and $\widetilde{d_2}$.

We also found that both prey and predator populations are decreased by rising prey harvesting $\widetilde{q}_1$, which may lead to extinction at high harvesting rates. Figures 7 and 8 illustrate how excessive harvesting destabilises the system, while increasing predator harvesting $\widetilde{q}_2$ lowers predator populations and permits prey to increase. The Hopf bifurcation in relation to the harvesting parameters is also depicted in Figures 9 and 10. Careful management of $\widetilde{q}_1$ and $\widetilde{q}_2$ is essential to maintain ecosystem stability and prevent species extinction.

Author contributions

The final document was typed, read, and approved by all authors, who each made an equal and substantial contribution to its creation.

Acknowledgements

Aziz Khan would like to thank Prince Sultan University for paying the APC and for the support through TAS research lab.

Conflict of interest

The authors declare no competing financial interest.

References

[1] Stoll M. Rachel Carson's *Silent Spring*, a book that changed the world. *Rachel Carson Center Virtual Exhibitions*. 2012. Available from: https://doi.org/10.5282/rcc/3517.

[2] Hallam TG, Clark CE. Non-autonomous logistic equations as models of populations in a deteriorating environment. *Journal of Theoretical Biology*. 1981; 93(2): 303–311. Available from: https://doi.org/10.1016/0022-5193(81)90106-5.

[3] Hallam TG, de Luna JT. Effects of toxicants on populations: a qualitative approach III. Environmental and food chain pathways. *Journal of Theoretical Biology*. 1984; 109(3): 411–429. Available from: https://doi.org/10.1016/S0022-5193(84)80090-9.

[4] Dubey B, Hussain J. A model for the allelopathic effect on two competing species. *Ecological Modelling*. 2000; 129(2–3): 195–207. Available from: https://doi.org/10.1016/S0304-3800(00)00228-3.

[5] Kar TK, Chaudhuri KS. On non-selective harvesting of two competing fish species in the presence of toxicity. *Ecological Modelling*. 2003; 161(1–2): 125-137. Available from: https://doi.org/10.1016/S0304-3800(02)00323-X.

[6] Samanta GP. A two-species competitive system under the influence of toxic substances. *Applied Mathematics and Computation*. 2010; 216(1): 291–299. Available from: https://doi.org/10.1016/j.amc.2010.01.061.

[7] Smith RH, Mead R. Age structure and stability in models of prey-predator systems. *Theoretical Population Biology*. 1974; 6(3): 308–322. Available from: https://doi.org/10.1016/0040-5809(74)90014-8.

[8] Muthaiah S, Baleanu D, Thangaraj NG. Existence and Hyers-Ulam type stability results for nonlinear coupled system of Caputo-Hadamard type fractional differential equations. *AIMS Mathematics*. 2021; 6(1): 168–194. Available from: https://doi.org/10.3934/math.2021012.

[9] Manivel M, Venkatesh A, Kumawat S. Numerical simulation for the co-infection of monkeypox and HIV model using fractal-fractional operator. *Modeling Earth Systems and Environment*. 2025; 11(3): 157. Available from: https://doi.org/10.1007/s40808-025-02359-2.

[10] Manivel M, Venkatesh A, Kumawat S. A comprehensive study of monkeypox disease through fractional mathematical modeling. *Mathematical Modeling and Numerical Simulation with Applications*. 2025; 5(1): 65–96. Available from: https://doi.org/10.53391/mmnsa.1571609.

[11] Saber S, Solouma E. Advanced fractional modeling of diabetes: bifurcation analysis, chaos control, and a comparative study of numerical methods Adams-Bashforth-Moulton and Laplace-Adomian-Padé method. *Indian Journal of Physics*. 2025; 99(13): 5151–5169. Available from: https://doi.org/10.1007/s12648-025-03712-y.

[12] Alhazmi M, Mirgani SM, Alahmari A, Saber S. Hybrid multi-step fractional numerical schemes for human-wildlife zoonotic disease dynamics. *AIMS Mathematics*. 2025; 10(9): 21126–21158. Available from: https://doi.org/10.3934/math.2025944.

[13] Yogeesh N, Mohammad SI, Divyashree J, Raja N, Vasudevan A, Long H. Pesticide residue induced hepatotoxicity: determination for animal studies based on fuzzy logic. *Applied Mathematics and Information Sciences*. 2025; 19(2): 365–378. Available from: http://dx.doi.org/10.18576/amis/190212.

[14] Farman M, Talib A, Nisar KS, Sambas A, Bayram M, Hafez M. Investigation of ABPV predict dynamics infection in honeybee colony production: soft patterns multiscale modeling with fractional approach. *Ain Shams Engineering Journal*. 2025; 16(10): 103626. Available from: https://doi.org/10.1016/j.asej.2025.103626.

[15] Caputo M, Fabrizio M. On the notion of fractional derivative and applications to the hysteresis phenomena. *Meccanica*. 2017; 52(13): 3043–3052. Available from: https://doi.org/10.1007/s11012-017-0652-y.

[16] Podlubny I. Geometric and physical interpretation of fractional integration and fractional differentiation. *arXiv:math/0110241*. 2001. Available from: https://doi.org/10.48550/arXiv.math/0110241.

[17] Kexue L, Jigen P. Laplace transform and fractional differential equations. *Applied Mathematics Letters*. 2011; 24(12): 2019–2023. Available from: https://doi.org/10.1016/j.aml.2011.05.035.

[18] Hammad HA, Aloraini NM, Abdel-Aty M. Existence and stability results for delay fractional differential equations with applications. *Alexandria Engineering Journal*. 2024; 92: 185–198. Available from: https://doi.org/10.1016/j.aej.2024.02.060.

[19] Li Y, Chen Y, Podlubny I. Stability of fractional-order nonlinear dynamic systems: Lyapunov direct method and generalized Mittag-Leffler stability. *Computers & Mathematics with Applications*. 2010; 59(5): 1810–1821. Available from: https://doi.org/10.1016/j.camwa.2009.08.019.

[20] Deshpande AS, Daftardar-Gejji V, Sukale YV. On Hopf bifurcation in fractional dynamical systems. *Chaos, Solitons & Fractals*. 2017; 98: 189–198. Available from: https://doi.org/10.1016/j.chaos.2017.03.034.

[21] Diethelm K. Efficient solution of multi-term fractional differential equations using P(EC)^{m}E methods. *Computing*. 2003; 71(4): 305–319. Available from: https://doi.org/10.1007/s00607-003-0033-3.

[22] Diethelm K, Ford NJ, Freed AD. A predictor-corrector approach for the numerical solution of fractional differential equations. *Nonlinear Dynamics*. 2002; 29(1): 3–22. Available from: https://doi.org/10.1023/A:1016592219341.

[23] Khan H, Abdel-Aty M, Almutairi DK, Gómez-Aguilar JF, Alzabut J. Artificial intelligence neural networking for data clustering of carbon dioxide model. *Ain Shams Engineering Journal*. 2025; 16(8): 103460. Available from: https://doi.org/10.1016/j.asej.2025.103460.

[24] Khan H, Alfwzan WF, Latif R, Alzabut J, Thinakaran R. AI-based deep learning of the water cycle system and its effects on climate change. *Fractal and Fractional*. 2025; 9(6): 361. Available from: https://doi.org/10.3390/fractalfract9060361.

[25] Khan H, Alzabut J, Tounsi M, Almutairi DK. AI-based data analysis of contaminant transportation with regression of oxygen and nutrients measurement. *Fractal and Fractional*. 2025; 9(2): 125. Available from: https://doi.org/10.3390/fractalfract9020125.

[26] Khan H, Alzabut J, Almutairi DK, Gulzar H, Alqurashi WK. Data analysis of fractal-fractional co-infection Covid-TB model with the use of artificial intelligence. *Fractals*. 2025; 33(4): 2540099. Available from: https://doi.org/10.1142/S0218348X25400997.

[27] Alqudah MA, Khan A, Mofarreh F, Abdeljawad T. Numerical results of fractional order difference system for norovirus disease with feedback neural networking. *Boundary Value Problems*. 2025; 2025(1): 179. Available from: https://doi.org/10.1186/s13661-025-02164-x.